Available online www.jsaer.com

***Journal of Scientific and Engineering Research*, 2024, 11(12):17-26**

Research Article

ISSN: 2394-2630
CODEN(USA): JSERBR

Experimental Study on The Propagation Law of Hydraulic Fractures in Shale with Fractures

Yapeng Zhang, Junqi Cui, Chen Feng, Nannan Wang, Zhixing Wei, Kai Wang

School of Safety Science and Engineering, Henan University of Technology, Jiaozuo 454003, China
Email：zhangyapeng0524@163.com

Abstract: The natural fractures at different spatial positions in shale can affect the propagation path of hydraulic fractures. Studying the influence mechanism of different forms of natural fractures on hydraulic fractures is of guiding significance for clarifying the mechanism of hydraulic fracture propagation and optimizing the fracture network. This article is based on the physical characteristics of the surrounding rock mainly composed of siltstone and mudstone in the Taiyuan Formation of the Carboniferous system. Similar materials are poured into rock samples to conduct hydraulic fracturing physical experiments. Based on a single fracture, the influence of different natural fractures on the initiation and expansion of hydraulic fractures is simulated; Using a single variable method, investigate the effects of natural fracture approximation angle and fracturing spacing on the initiation, propagation, and extension of hydraulic fractures. The results show that the larger the approximation angle, the more obvious the control effect of natural fractures on hydraulic fractures. When the approximation angle is 90 °, hydraulic fractures are more likely to pass through natural fractures and undergo turning and branching phenomena at the tip of natural fractures, which can easily form complex fracture networks. With the increase of fracturing spacing, the initiation pressure shows a trend of first decreasing and then increasing; The smaller the fracturing spacing and the larger the approach angle, the easier it is for natural fractures to be activated, and the greater the degree of deflection of hydraulic fractures. The research results have certain reference significance for improving the morphology of fracture networks and optimizing shale reservoir fracturing design.

Keywords: Natural fissures; Crack propagation; Hydraulic fracturing; Fracturing pressure.

1. Background

Hydraulic fracturing, also known as fracturing, is a technology used to enhance the productivity of oil and gas wells. Its fundamental principle involves injecting high-pressure fluid into wells to create fractures in the formation, thereby increasing channels for oil and gas flow and improving recovery rates. Hydraulic fracturing is primarily applied in the development of low-permeability oil and gas reservoirs and shale gas formations. Shale reservoirs feature deep burial depths, complex geological structures, high in-situ stress environments, and diverse thermal characteristics. These reservoirs are typically characterized by highly developed natural fractures that form complex fracture networks, enhancing reservoir permeability and providing primary pathways for fluid migration and storage. The gas production efficiency of a reservoir is closely related to the development of its natural fracture network, with the scale, distribution, and connectivity of the fractures directly affecting the production enhancement achieved through fracturing [1-3].

Shale reservoirs exhibit various types of natural fractures, including joints, faults, and bedding planes, which form during sedimentation and diagenesis. Due to subsequent burial pressure, these natural fractures are often closed and filled with cements such as carbonates, silicates, or clay minerals, reducing fracture permeability.

Reopening these cement-filled, closed fractures through hydraulic action is crucial for creating an effective fracture network during hydraulic fracturing [4-6].

The complex pore structure and low permeability of shale reservoirs often feature weak structural planes such as natural fractures, playing a critical role in shale gas migration and storage. To effectively connect natural fractures and form a high-efficiency, complex fracture network, large-scale hydraulic fracturing is typically employed. This technology applies high-pressure fluid to the reservoir, expanding weak structural planes and connecting them with artificial fracture networks, thereby enhancing reservoir permeability and significantly increasing shale gas recovery and production. The interaction between hydraulic and natural fractures leads to different fracture propagation paths, influencing the fracture network morphology. Understanding the impact of natural fractures on hydraulic fracture propagation is essential for optimizing the fracture network configuration.

Extensive research has been conducted on the effects of natural fractures on hydraulic fracture initiation pressure and propagation paths. Lv et al. [7] found through experiments that hydraulic fractures interacting with natural fractures at certain angles first activate and open the natural fractures before penetrating weaker matrix points. Chen Mian et al. [8] studied factors affecting fracture propagation, including the dip angle of natural fractures, approach angle, and horizontal stress difference, proposing a new failure criterion for predicting fracture propagation. Hu et al. [9-11] used glass plates to simulate interactions between hydraulic and natural fractures, observing fracture termination, deflection, or penetration, with smaller approach angles favoring fracture deflection.

Further research by Zhao Haifeng et al. [12] revealed shear-slip effects induced by hydraulic-natural fracture interactions, enhancing fracture conductivity. Zhang Kuangsheng et al. [13] established a multi-scale porous imbibition model considering fluid pressure and proposed a new concept of fracture network swept volume coefficient, quantitatively evaluating fracture network swept volume and indicating that shale oil fractures often form strip-like networks resembling "cacti." Key factors influencing the swept volume include fracturing fluid volume, fracture density, brittleness index, operational flow rate, horizontal stress difference, reservoir thickness, and proppant addition.

Shen Yongxing et al. [14] conducted hydraulic fracturing physical simulations on shale reservoirs using a twodimensional fluid-solid coupling fracture propagation model, studying the effects of horizontal stress difference, natural fracture intersection angle, and length on fracture propagation. Results indicated a linear increase in fracturing initiation pressure with increasing horizontal stress difference, providing valuable experimental insights into hydraulic fracture propagation mechanisms and interactions with natural fractures.

Hou Mengru [15] developed a shale microstructure model considering mineral interface effects, revealing hydraulic fracture propagation patterns influenced by these effects. Dong Yan [16] systematically studied the mechanisms of hydraulic-natural fracture intersection, complex fracture network formation, and the impact of reservoir anisotropy on fracturing processes, proposing an equivalent evaluation method for reservoir fracturing transformation. Zhang Xuancheng et al. [17-19] investigated the impacts of fracturing fluid properties, reservoir characteristics, and pore overpressure on fracturing efficiency.

Su Yunlei et al. [20-22] studied optimal hydraulic fracturing designs for shale reservoirs, including stage spacing, cluster spacing, fluid volume, and operational flow rate. Deng Jiaqi [23] analyzed factors affecting the accuracy of artificial fracture characterization through post-fracture network simulations and numerical modeling, enhancing prediction accuracy by adjusting parameter sensitivities. Ge Shuaishuai et al. [24] demonstrated that hydraulic roof cutting can effectively weaken hard roof strength and reduce mine pressure manifestations. Borehole observations showed significantly increased inner wall fractures post-fracturing, indicating good hydraulic fracturing performance.

Current research mainly focuses on the intersection criteria between hydraulic fractures and pre-existing fractures, with limited studies on how spatial variations affect interactions. The lack of comprehensive investigation into spatially varying interactions constrains the understanding of fracture propagation behaviors. Therefore, systematic research on spatial variations' impact on hydraulic-natural fracture interactions has significant academic and practical value. Most studies consider approach angles of 30°, 45°, and 60°, with limited research on larger angles. Experimental specimens are typically large outcrop rock samples, making it challenging to observe fracture surfaces. This study uses water with fluorescent tracers as the fracturing fluid, reconstructing fracture surfaces in 3D to analyze the effects of varying approach angles and fracture spacings on

hydraulic fracture initiation and propagation, enhancing the theoretical framework of shale gas hydraulic fracturing.

2. Experimental System Experimental Equipment

This experiment uses a true triaxial gas-containing coal sample fracturing test system independently developed by the research team. The system consists of four modules: the main body, the stress loading subsystem, the fracturing fluid injection subsystem, and the monitoring and control subsystem, as shown in Figure 1. The main body includes a chamber capable of holding samples with dimensions up to 300(±5)mm × 200(±5)mm × 200(±5)mm. The stress loading subsystem includes three independent double-plunger hydraulic metering pumps, each of which can apply stress to one of the three axial ends. The flow rate range is [1,66] mL/min, with a flow rate repeatability of no more than 0.1% (1 mL/min), and the maximum working pressure is 50 MPa. The core component of the fracturing fluid injection subsystem is the KD-250 dual-cylinder constant-speed, constantpressure pump, with a flow rate range of [0,50] mL/min and a maximum working pressure of 60 MPa. It supports three different injection modes: constant flow, constant pressure, and tracking. The monitoring and control subsystem is responsible for recording parameters such as axial and injection pressures, as well as fracturing time, throughout the entire fracturing process. This equipment is capable of realistically simulating the in-situ stress conditions of deep strata and meeting the requirements for fracturing operations.

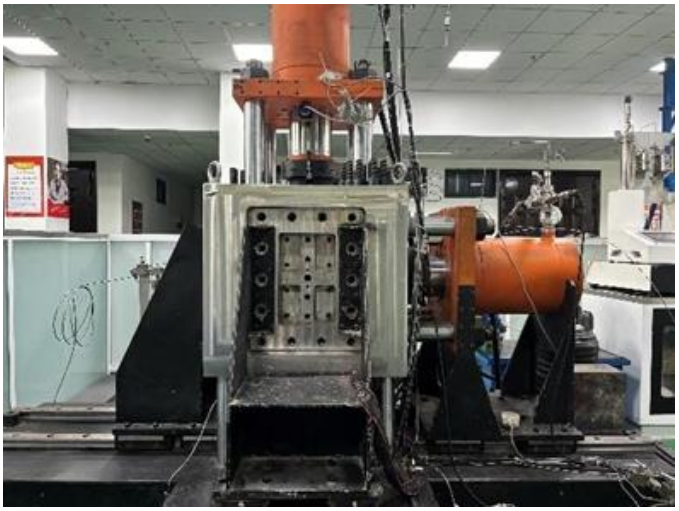

Figure 1: Schematic diagram of the true triaxial gas containing coal sample fracturing test system

Sample Preparation

The samples prepared for this experiment have dimensions of 200mm × 200mm × 300mm. To simulate natural fractures at different spatial locations, self-made prefabricated fractures were selected and embedded into the samples. During the sample preparation process, similar materials were used to substitute shale. The samples were cast using a mixture of silicate cement and fine sand with a particle size smaller than 2mm, with a mixing ratio of 3:2:0.5 (fine sand:cement:water). After casting, the molds were removed 48 hours later, and during the curing period, the temperature and humidity of the samples were kept constant. The curing period lasted for 28 days. The mechanical properties of the samples are shown in Table 1.

Table 1: Basic Mechanical Parameters of Samples

Mechanical Parameters	Elastic Modulus	Uniaxial Compressive Strength	Poisson's Ratio
Average Value	11.239GPa	26.129MPA	0.115

Prefabricated fractures were simulated using corrugated boards, a simple method that effectively replicates natural fractures. The paper strips were vertically placed along the diagonal of the sample, with the bottom edge aligned with the water injection point at the same horizontal level. The paper strips have a length of 6 cm, a width of 2 cm, and a thickness of 2 mm. The embedding depth was kept constant, and different approach angles

(30°, 60°, 90°) and fracturing spacings (1 cm, 3 cm, 5 cm) were set. The schematic diagram of the rock sample structure is shown in Figure 2.

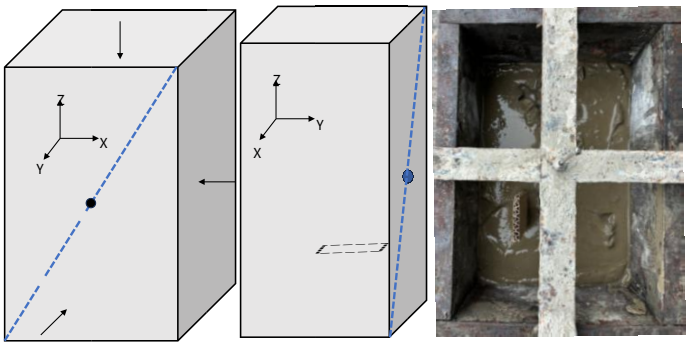

Figure 2: Schematic diagram of rock sample structure

Experimental Scheme

To investigate the effects of different natural fracture approach angles and fracturing spacings on hydraulic fracturing, a detailed analysis was conducted on the crack initiation pressure, fracture surface characteristics, and the propagation patterns of the fracturing cracks. The approach angle is defined as the angle between the prefabricated fractures and the direction of the maximum horizontal stress. Before the experiment, a yellow tracer dye was added to the fracturing fluid to facilitate the observation and analysis of the fracture propagation. The injection rate was set to 30 mL/min, and throughout the experiment, both injection pressure and volume were monitored. When the injection pressure curve began to consistently decrease, fluid injection was continued for one more minute to ensure complete expansion of the hydraulic fracture inside the sample. After the experiment, the sample was removed, and the water-stained areas were examined to determine the propagation path, shape, and extent of the hydraulic fractures. Key coordinates along the fracture propagation path were extracted, and the fracturing surface during the "point-line-surface-volume" propagation process was reconstructed. The experimental scheme is shown in Table 2.

Table 2: Hydraulic Fracturing Experimental Plan

Sample ID	Injection Rate mL/min	Angle θ/°	Spacing D/mm	Triaxial Loading Stress （MPA)		
				σH	σh	σv
R-1			10			
R-2		30	30			
R-3			50			
R-4			10			
R-5	30	60	30	8	4	6
R-6			50			
R-7			10			
R-8		90	30			
R-9			50			

3. Experimental Results and Analysis of Hydraulic Fracture Propagation Characteristics

The surface crack patterns of the samples are summarized in Figure 3. To more intuitively display the impact of natural fracture locations and angles on the propagation of hydraulic fractures, the key coordinate points on the surface of the sample after fracture propagation were extracted, and the fracturing surface was reconstructed, as shown in Figure 4.

To study the interaction between hydraulic fractures and natural fractures, a physical experimental approach was used to investigate the effect of fracturing spacing and approach angle parameters on the intersection of hydraulic and natural fractures. Three sets of experiments were conducted, with each set containing three samples. The spacing was varied between groups, while the approach angle was varied within each group.

To investigate the interaction between hydraulic fractures and natural fractures, a physical experimental approach was employed to explore the effect of fracturing spacing and approach angle parameters on the intersection of hydraulic fractures with natural fractures. A total of three sets of experiments were conducted, with each set consisting of three samples. Fracturing spacing was varied between the groups, while approach angle was varied within each group.

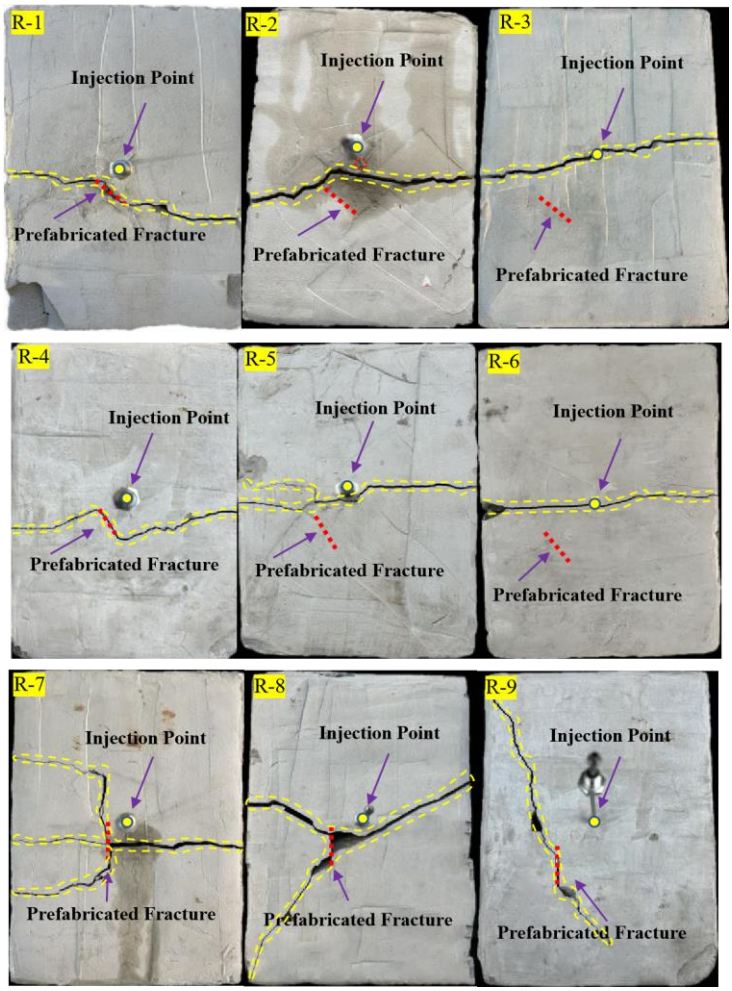

Figure 3: Summary of Water Pressure Cracks

The results of the experiments are analyzed as follows:

a. R-1: The hydraulic fracture intersected with the prefabricated fracture and then changed direction. The direction of the change was consistent with the direction of the prefabricated fracture.

b. R-2: The hydraulic fracture did not intersect with the prefabricated fracture, but a direction change occurred only on one side of the prefabricated fracture. The direction of change was opposite to the direction of the prefabricated fracture.

c. R-3: The hydraulic fracture did not intersect with the prefabricated fracture, and the fracture plane tilted overall, with the tilt direction pointing towards the tip of the prefabricated fracture.

d. R-4: The hydraulic fracture was initially captured by the prefabricated fracture. The hydraulic fracture intersected with the prefabricated fracture but could not penetrate it. Stress concentrated at the fracture tip, leading to a double-direction change along the fracture tip.

e. R-5: The hydraulic fracture changed direction and bifurcated near the tip of the prefabricated fracture, forming secondary fractures. These secondary fractures extended vertically along the Z-axis, with the direction of the change aligned with the maximum horizontal principal stress.

f. R-6: The hydraulic fracture initiated from the injection point and expanded along the plane of the maximum horizontal principal stress, extending to the boundary.
g. R-7: The hydraulic fracture penetrated the prefabricated fracture and opened along the tip of the prefabricated fracture, forming a "cross" shape.
h. R-8: After entering the prefabricated fracture, the main fracture only penetrated through one side and opened along the tip of the prefabricated fracture before deflecting, forming a "Y" shaped fracture.
i. R-9: No visible fracture was generated in the X-axis direction. The hydraulic fracture extended along the direction of the prefabricated fracture tip in the Z-axis, with one wing shifting towards the X-axis. After extending for a certain distance, it stagnated without reaching the boundary.

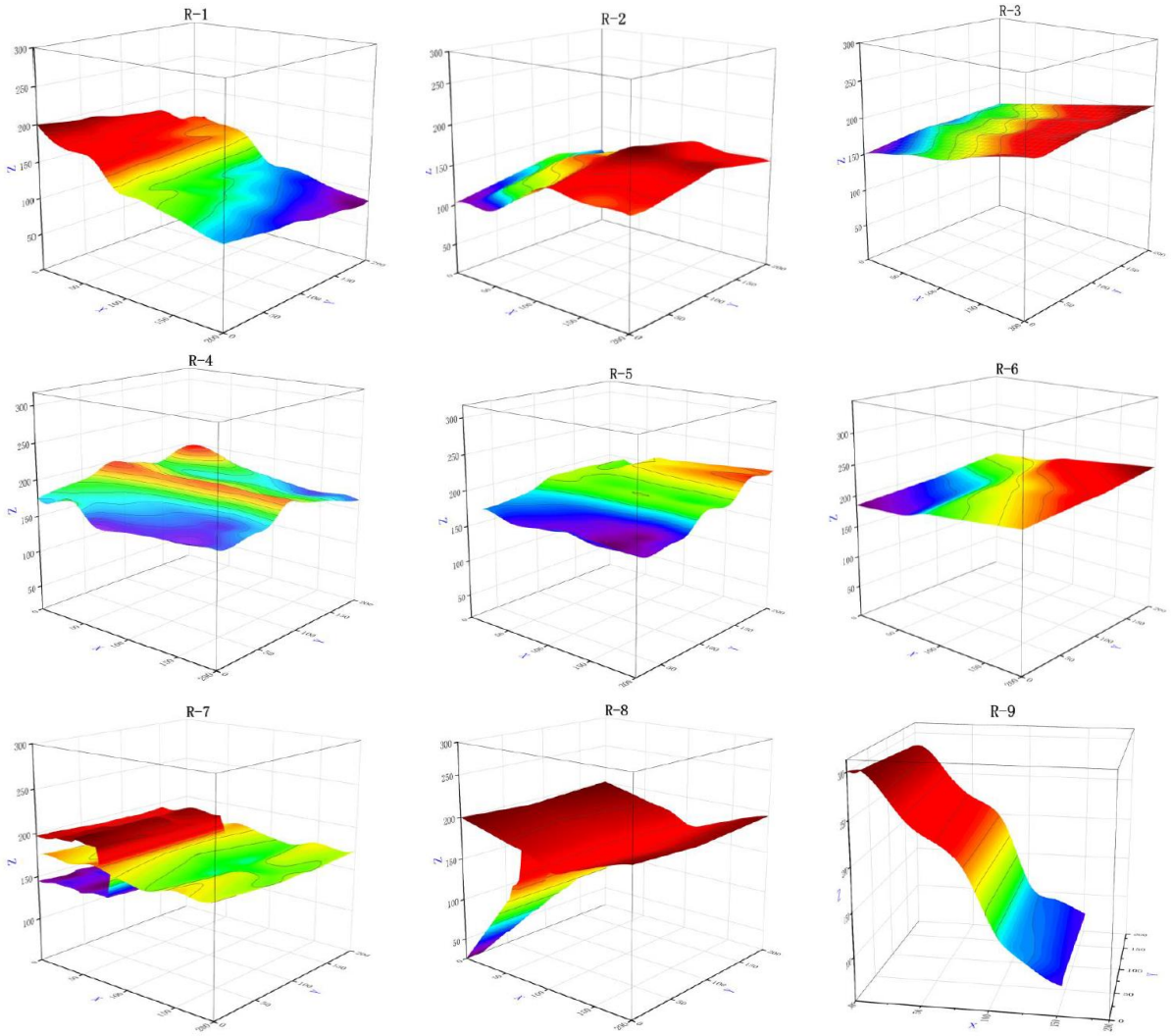

Figure 4: Reconstruction of Sample Cross Section

Hydraulic fractures may exhibit deflection, opening, or intersection after extending a certain distance along natural fractures. Specifically, when hydraulic fractures interact with natural fractures, three types of intersection modes can occur: the hydraulic fracture may deflect after encountering the natural fracture, directly open and develop along the direction of the natural fracture, or cross through the natural fracture. To further analyze these intersection modes, Sample 9, Sample 4, and Sample 7 represent these three scenarios, as shown in Figure 3. In the figure, the yellow lines represent hydraulic fractures, the yellow circles indicate injection points, and the red lines represent prefabricated fractures.

From Figure 3, it can be observed that samples containing small-angle natural fractures (30°, 60°) generally exhibit tensile failure (Samples 1-6). When the approach angle is 90°, the failure modes of the samples are more complex, including both tensile and shear failure (Samples 7 and 8), or shear failure alone (Sample 9).

Analysis of Influencing Factors

a. Approach Angle of Natural Fracture

By comparing R-1, R-4, and R-7, it can be observed that the approach angle of the natural fracture has a significant impact on the hydraulic fracture. Specifically, as the approach angle decreases, it becomes more difficult for the hydraulic fracture to penetrate the natural fracture. In this case, the natural fracture is more likely to open. When the approach angle is 30°, the hydraulic fracture continues to expand along the direction of the natural fracture. At 60°, the hydraulic fracture opens within the natural fracture but then deflects, no longer extending along the fracture tip. The direction of deflection aligns with the direction of maximum stress. When the natural fracture is perpendicular to the direction of maximum stress, the hydraulic fracture penetrates the natural fracture and continues to expand, extending along the Z-axis at the tip of the natural fracture. It then deflects under the influence of the maximum stress.

b. Fracturing Spacing

The closer the natural fracture is to the injection point, the easier it is for the fracturing fluid to enter the natural fracture, thereby activating and stimulating the natural fracture. As the spacing increases, the influence of the stress field at the tip of the natural fracture on the hydraulic fracture propagation gradually weakens. At a spacing of 10 mm, when the hydraulic fracture encounters the natural fracture, the fracture either opens, deflects, or is penetrated. At 30 mm, the hydraulic fracture deflects near the tip, with the direction of deflection varying significantly: under low approach angles, it deflects towards the tip, while at 60°, it deflects in the opposite direction, and at 90°, a double deflection occurs. As the spacing increases, the influence of the natural fracture gradually diminishes, and the hydraulic fracture becomes primarily aligned with the maximum principal stress, forming a main fracture. At high approach angles and large distances, the influence of the natural fracture is minimized. As seen in Sample 9, after the hydraulic fracture enters the natural fracture, it does not penetrate the fracture or exhibit significant deflection. The natural fracture opens, and the hydraulic fracture extends along the fracture tip for a short distance before undergoing a slight deflection.

For Sample R-2, the hydraulic fracture initiates at the injection point and extends along the -Y axis. It deflects at the tip of the prefabricated fracture, with the direction of deflection differing from the horizontal maximum principal stress direction. The deflection forms a 30° angle with the horizontal direction, extending towards the boundary, while the other wing of the hydraulic fracture extends towards the X-axis direction.

In summary, under smaller approach angles (such as 30° and 60°), the differences in physical properties and the induced stress of the prefabricated fractures cause the hydraulic fracture to deflect in one wing towards the interface, while the other wing deviates and extends towards the boundary. The hydraulic fracture generally trends towards the maximum stress direction, and the control effect of horizontal stress on the hydraulic fracture is stronger than the induced stress of the prefabricated fracture.

At the same approach angle, the complexity of the hydraulic fracture decreases as the fracturing spacing increases. When the fracturing spacing is 10 mm, the fracturing fluid enters the prefabricated fracture, opening along the fracture tip. After expanding a certain distance, the fracture continues to extend towards the boundary along the direction of the maximum principal stress. At the other two spacings, the hydraulic fracture gradually deviates from the prefabricated fracture, with the influence of the prefabricated fracture decreasing, and the fracture pattern tends to become more uniform.

When the fracturing spacing is fixed, the larger the approach angle, the stronger the tendency for the hydraulic fracture to pass through the prefabricated fracture. This is more favorable for the deflection of the hydraulic fracture and the formation of secondary fractures, leading to the development of more complex fracture networks. However, under high approach angles, the fracturing fluid energy tends to accumulate at the fracture tip, causing the width of the main fracture to decrease and the potential energy to diminish. Because the prefabricated fracture is perpendicular to the maximum stress direction, the fracturing fluid is more likely to enter the fracture at high approach angles. The activation degree of the prefabricated fracture is related to the fracturing spacing: the smaller the spacing, the better the activation effect of the prefabricated fracture. In contrast, the larger the fracturing spacing, the simpler the hydraulic fracture becomes.

Analysis of Pumping Pressure Curve Characteristics

The rise and fall characteristics of the pumping pressure curve during fracturing can effectively reflect the propagation of hydraulic fractures [26, 27]. To further investigate the deflection patterns of hydraulic fractures under the influence of material property differences and the interaction between fractures, the pressure-time curves for samples under different conditions were plotted, along with the morphological features of the hydraulic fractures (see Figure 5). Based on the variation in pumping pressure, the pressure-time curve can be divided into the following four stages:

a. Fracturing Fluid Filling Stage: In this stage, the fracturing fluid fills the pipeline and fracturing tubes, but there is no injection into the rock matrix. Therefore, the change in pumping pressure is minimal.

b. Fracture Initiation Stage: After the fracturing fluid is injected, the pressure in the fracturing chamber rises quickly to its peak value after reaching a shut-in pressure. The peak pressure corresponds to the initiation pressure of the rock formation. Subsequently, fracture propagation enters Stage III.

c. Fracture Propagation Stage: Under continued fracturing fluid injection, the pressure decreases rapidly and then stabilizes. Once new fractures are formed, the fracturing fluid fills the fracture space, and after a short period of shut-in pressure, the fracture initiates again, further propagating. In this stage, the pressure exhibits fluctuations, with more significant oscillations in formations with higher brittleness.

d. Fracture Penetration Stage: With continued fracturing fluid injection, the fracture extends to the boundary and penetrates the sample, leading to complete failure. At this point, the fracturing fluid flows out, and the integrity of the hydraulic fracture is compromised, losing the shut-in pressure and initiation conditions, followed by a sharp pressure drop.

As shown in Figure 5, all fracturing operations with different fracturing spacings went through four stages, and the overall pressure variation trend is roughly the same. Local differences are mainly concentrated in the fracture initiation stage (Stage II) and the fracture propagation stage (Stage III). The characteristic pressure values for each stage are listed in Table 3. From Figure 5, it can be observed that, under approaching angles of 30° and 60°, the variation in fracturing spacing primarily affects the initial fracture initiation pressure. For the same angle, as the fracturing spacing increases, the initial fracture initiation pressure also increases. Additionally, as the fracturing spacing increases, the time required for the sample to transition from fracture initiation to complete fracture extension gradually decreases.

Table 3: Stage Characteristics of Pump Injection Pressure

Sample Number	Fracture Initiation Pressure (MPa)	Propagation Pressure (MPa)	StageI (s)	StageII (s)	StageIII (s)	StageIV (s)	End Time (s)
R-1	5.78	4.92	20	21	148	17	206
R-2	7.03	5.90	25	27	104	23	179
R-3	11.35	8.00	21	20	108	19	168
R-4	6.91	6.10	15	25	163	40	243
R-5	8.86	5.90	17	32	132	53	234
R-6	11.45	6.10	18	40	131	35	224
R-7	7.45	6.18	10	25	125	56	216
R-8	7.62	5.36	9	30	166	49	254
R-9	11.70	9.12	12	33	168	47	260

When the approaching angle is 30°, increasing the fracturing spacing also increases the pressure required for fracture propagation. However, when the approaching angle is 60°, the increase in fracturing spacing has no significant effect on the fracture propagation pressure. Under high approaching angles, the variation in fracturing spacing does not significantly affect either the initiation pressure or the propagation pressure. At this stage, the change in fracturing spacing has a more considerable impact on Stage II. As the fracturing spacing increases, the time required for fracture initiation increases. Unlike low approaching angles, under these conditions, the time for sample fracture increases with increasing fracturing spacing. This is because, at low

approaching angles, the degree of sample fracture and the extent of fracture propagation become more uniform as the fracturing spacing increases.

At large angles, the hydraulic fracture is activated at the junction of the pre-existing fracture tip, which requires more energy. This leads to longer fracturing fluid injection times and longer experiment durations. For the same fracturing spacing, as the approaching angle increases, the fracture initiation pressure gradually stabilizes. At a spacing of 10mm, the difference in fracture initiation pressure is +1.13 MPa and +0.54 MPa; at 30mm, the difference is +1.83 MPa and -1.24 MPa; and at 50mm, the initiation pressure is +0.10 MPa and +0.25 MPa.

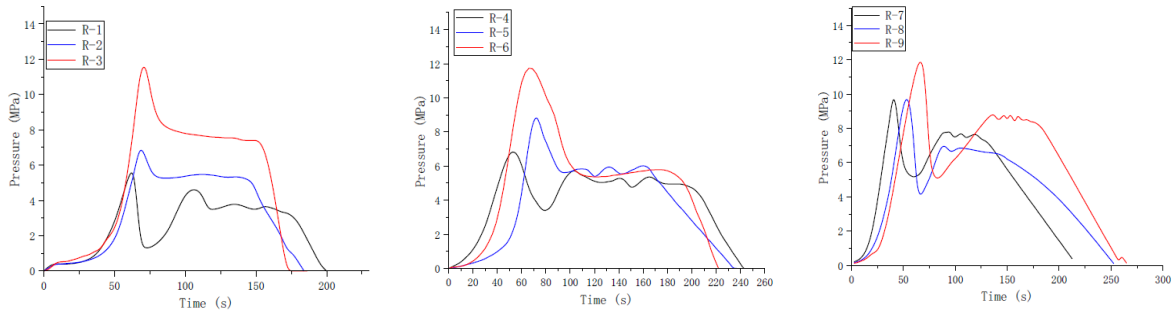

Figure 5: Sample pressure time curve

4. Conclusion

a. The interaction between hydraulic fractures and natural fractures mainly results in three outcomes: opening, deflection, and crossing. When the approaching angle is small (such as 30° or 60°), the hydraulic fracture is more likely to open along the direction of the natural fracture tip or deflect near the tip and ultimately tend toward the direction of the maximum horizontal principal stress. As the fracture spacing increases, the fracture surface gradually becomes smoother. In contrast, with a larger approaching angle, the hydraulic fracture is more likely to cross the natural fracture, making the fracture propagation path more complex. When the natural fracture is perpendicular to the maximum horizontal principal stress, the hydraulic fracture will form a "cross" or "Y" shaped fracture after crossing the natural fracture. In cases with a smaller angle, the overall fracture tends to form a "linear" shape, with one wing intersecting or deflecting toward the natural fracture and the other wing deflecting away.

b. As the fracture spacing increases, the difficulty of initiating a fracture increases, and the expansion behavior of the hydraulic fracture in the XOY plane becomes more pronounced. Near the injection point, an increase in fracture spacing significantly raises the initiation pressure. However, as the fracture spacing continues to increase, this effect gradually diminishes, and the initiation pressure tends to become consistent across different approaching angles. When the approaching angle is 30°, the increase in fracture spacing not only leads to a higher initiation pressure but also causes the propagation pressure of the hydraulic fracture to gradually increase. In contrast, at 60° and 90°, the change in propagation pressure of the hydraulic fracture is not significant.

c. Natural fractures play a guiding role to some extent. The smaller the approaching angle, the better the guiding effect; however, natural fractures are less likely to be activated, and the hydraulic fractures have difficulty penetrating them. In contrast, when the approaching angle is close to 90°, hydraulic fractures are more likely to penetrate the natural fractures, and the secondary fractures at the intersection become more complex.

References

[1]. Yan K., Lei Q.S. (2021). The exploration and development prospects of unconventional oil and gas resources in China - Review of "Petroleum Refining Engineering". China Nonferrous Metals, 50(06): 118.

[2]. Wang D.R. (2018). Achievements and prospects of natural gas development in China - Interview with Academician Zou Cailin of the Chinese Academy of Sciences. Petroleum Knowledge, 2018(04): 6-7.

[3]. Zhang Y.J., Sun W.H., Wu J. (2013). Survey of the exploration and development progress of shale gas and its prospect analysis. Science and Technology Innovation and Application, 2013(10): 88.

[4]. Cheng Y.S. (2024). Discrete element numerical simulation study on the anisotropic shale hydraulic fracture propagation law. Liaoning University of Engineering and Technology.
[5]. Guo J.Y., Wang Y. (2018). Study on the mechanism of hydraulic fractures connecting natural fractures and activating their extension. Journal of Engineering Geology, 26(06): 1523-1533.
[6]. Liu W., Cao X.P., Xu Y.D., et al. (2023). Production data analysis and capacity evaluation methods for shale oil wells. Fault Block Oil & Gas Fields, 30(04): 572-578.
[7]. Lv H.Y., Cheng Z.B., Liu F. (2021). Study on the mechanism of a new fully mechanical mining method for extremely thick coal seams. International Journal of Rock Mechanics and Mining Sciences, 142.
[8]. Chen M., Pang F., Jin Y. (2000). Large-size true triaxial hydraulic fracturing simulation and analysis. Journal of Rock Mechanics and Engineering, (S1): 868-872.
[9]. Cheng Q.Y., Huang B.X., Shao L.Y., et al. (2020). Combination of pre-pulse and constant pumping rate hydraulic fracturing for weakening hard coal and rock mass. Energies, 13(21).
[10]. Deng J.Q., Lin C., Yang Q., et al. (2016). Investigation of directional hydraulic fracturing based on true triaxial experiment and finite element modeling. Computers and Geotechnics, 75.
[11]. Wang J.H., Yu B., Kang H.P., et al. (2015). Key technologies and equipment for fully mechanized top-coal caving operation with a large mining height at ultra-thick coal seams. International Journal of Coal Science & Technology, 2(2).
[12]. Zhao H.F., Chen M., Jin Y., et al. (2012). Rock fracture dynamics of shale gas reservoir network fracture system. Petroleum Exploration and Development, 39(04): 465-470.
[13]. Zhang K.S., Xue X.J., Tao L., et al. (2023). New methods and applications for volume fracturing network evaluation in shale oil horizontal wells. Special Oil & Gas Reservoirs, 30(05): 127-134.
[14]. Shen Y.X., Feng Z.C., Zhou D., et al. (2021). Numerical simulation study on the influence of natural fractures on hydraulic fracture propagation in shale reservoirs. Coal Science and Technology, 49(08): 195-202.
[15]. Hou M.R., Liang B., Sun W.J., et al. (2023). Study on the impact of mineral interface stiffness on shale hydraulic fracture propagation. Oil and Gas Reservoir Evaluation and Development, 13(01): 100-107.
[16]. Dong Y. (2023). Numerical simulation of complex hydraulic fracture networks and fracture effectiveness evaluation. University of Science and Technology of China.
[17]. Zhang X.C. (2023). Effect of fluid retention on rock physical properties in shale reservoirs. Xi'an Petroleum University.
[18]. Xiong Z.L. (2023). Overpressure mechanism and prediction methods for shale gas reservoirs. China University of Petroleum (Beijing).
[19]. Wang L. (2023). Reservoir physical characteristics and surfactant-enhanced oil recovery mechanisms in shale oil reservoirs. China University of Petroleum (Beijing).
[20]. Zhang S.P. (2023). Deep shale oil reservoir fracture propagation simulation and construction parameter optimization. China University of Petroleum (Beijing).
[21]. Su Y.L. (2023). Complex fracture network fracturing simulation and design application in shale reservoirs. China University of Petroleum (Beijing).
[22]. Wang W.C. (2023). Comprehensive evaluation and intelligent perforation cluster selection method for shale oil reservoirs. China University of Petroleum (Beijing).
[23]. Deng J.Q. (2024). Research on improving the prediction accuracy of artificial fractures in horizontal wells for shale gas reservoirs. Journal of Jianghan Petroleum College, 37(02): 26-29.
[24]. Ge S.S., Sun L., He L.F., et al. (2024). Study on segmented hydraulic fracturing unloading technology for mining hard roof in comprehensive coal mining. Mining Research and Development, 44(07): 165-173.
[25]. Hu Q.T., Liu J.C., Li Q.G., et al. (2022). Numerical simulation of induced stress field for coal seam segmented hydraulic fracturing seepage. Journal of Mining and Safety Engineering, 39(04): 761-769.
[26]. Liang T.C., Liu Y.Z., Fu H.F., et al. (2018). Experimental study on multi-stage cyclic pumping hydraulic fracturing. Geotechnical Mechanics, 39(S1): 355-361.